Molecular Biology of the Cell
Vol. 20, 2549–2562, May 15, 2009

Plastin 1 Binds to Keratin and Is Required for Terminal Web Assembly in the Intestinal Epithelium

Eva-Maria S. Grimm-Günter,*†‡ Céline Revenu,‡§‖ Sonia Ramos,*¶ Ilse Hurbain,§ Neil Smyth,# Evelyne Ferrary,@ Daniel Louvard,§ Sylvie Robine,§ and Francisco Rivero*†

*Center for Biochemistry, Medical Faculty, University of Cologne, D-50931 Cologne, Germany; †Centre for Biomedical Research, The Hull York Medical School and Department of Biological Sciences, University of Hull, Hull HU6 7RX, United Kingdom; §Unité Mixte de Recherche 144, Centre National de la Recherche Scientifique/Institut Curie, F-75248 Paris, France; #School of Biological Sciences, University of Southampton, Southampton SO1 6PX, United Kingdom; and @Unité 867 Institut National de la Santé et de la Recherche Médicale/Université Paris Diderot-Paris 7, Faculté Xavier Bichat, F-75870 Paris, France

Submitted October 14, 2008; Revised February 17, 2009; Accepted March 12, 2009
Monitoring Editor: Thomas D. Pollard

Plastin 1 (I-plastin, fimbrin) along with villin and espin is a prominent actin-bundling protein of the intestinal brush border microvilli. We demonstrate here that plastin 1 accumulates in the terminal web and interacts with keratin 19, possibly contributing to anchoring the rootlets to the keratin network. This prompted us to investigate the importance of plastin 1 in brush border assembly. Although in vivo neither villin nor espin is required for brush border structure, plastin 1-deficient mice have conspicuous ultrastructural alterations: microvilli are shorter and constricted at their base, and, strikingly, their core actin bundles lack true rootlets. The composition of the microvilli themselves is apparently normal, whereas that of the terminal web is profoundly altered. Although the plastin 1 knockout mice do not show any overt gross phenotype and present a normal intestinal microanatomy, the alterations result in increased fragility of the epithelium. This is seen as an increased sensitivity of the brush border to biochemical manipulations, decreased transepithelial resistance, and increased sensitivity to dextran sodium sulfate-induced colitis. Plastin 1 thus emerges as an important regulator of brush border morphology and stability through a novel role in the organization of the terminal web, possibly by connecting actin filaments to the underlying intermediate filament network.

INTRODUCTION

Columnar enterocytes are the most abundant cell population of the intestinal epithelium. Their apical brush border (BB) consists of an exquisitely regular array of cell surface projections, the microvilli (MV) (Mooseker, 1985). Each microvillus is supported by a densely packed bundle of actin filaments that extends into the apical part of the cytoplasm, the so-called terminal web (TW), in which it is referred to as the rootlet. The axial bundles are extensively cross-linked by plastin 1 (also called I-plastin, I-fimbrin, or simply fimbrin) (Bretscher and Weber, 1980), villin (Bretscher and Weber, 1979), and the small splicing variant of espin (Bartles *et al*., 1998) and are attached to the plasma membrane by class I myosins (Heintzelman *et al*., 1994) and ezrin (Bretscher, 1983). In the TW region, the actin bundles are stabilized by tropomyosin, interconnected by myosin II and spectrin and linked to the junctional complex and the keratin network (Bement and Mooseker, 1996).

The enterocytes differentiate from proliferating cells in the crypt region of the intestinal mucosa and migrate toward the tip of the villus, from which they are shed 2 to 7 d later (Crosnier *et al*., 2006). Crypt cells already possess short MV, but lack a mature TW. On enterocyte maturation, the length and density of MV increase and the TW becomes assembled (Fath *et al*., 1990). Most of the main cytoskeletal components of the BB were identified >20 y ago, and their actions at the molecular level are fairly well understood (Bement and Mooseker, 1996). However, we lack a complete picture of how the BB is assembled and the individual contributions of each component. Studies addressing these questions in situ have been hampered by the inaccessibility and complexity of the intestine, leading to the development of two approaches. The first approach uses cell lines capable of forming polarized monolayers that display morphological features resembling those of enterocytes. For example, down-regulation of villin using an antisense approach resulted in altered development of a BB in Caco2 cells (Costa de Beauregard *et al*., 1995), whereas overexpression of espin or villin caused increased MV length in LLC-PK1 cells (Arpin *et al*., 1994; Loomis *et al*., 2003). Such studies cannot reproduce the sit-

This article was published online ahead of print in *MBC in Press* (http://www.molbiolcell.org/cgi/doi/10.1091/mbc.E08–10–1030) on March 25, 2009.

‡ These authors contributed equally to this work.

Present addresses: ‖ European Molecular Biology Laboratory, Department of Cell Biology and Biophysics, Meyerhofstrasse 1, 69126 Heidelberg, Germany; ¶ Instituto del Frío, Consejo Superior de Investigaciones Científicas, José Antonio Novais 10, Ciudad Universitaria, 28040 Madrid, Spain.

Address correspondence to: Francisco Rivero (francisco.rivero@hyms.ac.uk).

Abbreviations used: BB, brush border; DSS, dextran sodium sulfate; MV, microvilli; TW, terminal web.

uation in vivo. In fact, studies on knockout mice models demonstrate that none of several components is required for the formation of the MV, although in some cases the resulting structures reveal variable degrees of morphological and compositional alterations. Targeting of the ezrin gene results in mice that do not survive past weaning and display abnormal villus morphogenesis. Although enterocytes develop a BB, MV are short and irregular (Saotome *et al*., 2004). Mice deficient in myosin 1a lack an overt phenotype at the whole animal level, but closer examination revealed defects in BB organization and in the composition of the MV. This limited phenotype was attributed to compensation by another myosin 1 isoform (myosin 1c) usually absent from the BB (Tyska *et al*., 2005). Also, targeting of single keratin genes (K8, K18, and K19) has not revealed major alterations in those studies in which the gut has been examined (Baribault *et al*., 1994; Magin *et al*., 1998; Tamai *et al*., 2000; Ameen *et al*., 2001), possibly because of compensation by another keratin of the same class.

Although in vitro studies postulated a leading role for villin in the assembly of MV, disruption of the mouse villin gene does not alter the ultrastructure of the MV or the localization of actin-binding or membrane proteins (Pinson *et al*., 1998; Ferrary *et al*., 1999), albeit mice seem more sensitive to induced colitis (Ferrary *et al*., 1999). Functional redundancy with other actin-bundling proteins, namely, espin and plastin 1, may explain the mild phenotype of the villin-deficient mice. A spontaneous espin mutant mouse (the deaf jerker mouse) has hearing loss with degenerating stereocilia of auditory cells (Zheng *et al*., 2000) but does not show any morphological alteration in the intestinal epithelia (Revenu and Robine, unpublished data).

There is little information as to the role of plastin in BB morphogenesis (Lin *et al*., 1994; Loomis *et al*., 2003). Plastins are conserved from lower eukaryotes to human (Delanote *et al*., 2005). In mammals, three plastins are expressed in a cell–type-specific manner, each encoded by a different gene (Lin *et al*., 1993). Plastin 1 (encoded by the *Pls1* gene) is specifically expressed in the small intestine, colon, and kidney (Lin *et al*., 1994) as well as in stereocilia of the inner ear cells (Tilney *et al*., 1989). Plastin 2 (L-plastin) is expressed in cells of the hematopoietic lineage but becomes expressed in tumor cells of nonhematopoietic origin (Lin *et al*., 1988), and it is important for integrin activation (Chen *et al*., 2003). Plastin 3 (T-plastin) is present in diverse cell lineages, localizes at the leading edge and focal contacts of mesenchymal cells (Arpin *et al*., 1994) and transiently in stereocilia (Daudet and Lebart, 2002) and intestinal MV (Chafel *et al*., 1995) and has a stabilizing effect on actin filaments (Giganti *et al*., 2005).

The observations that plastin 1 accumulates in the TW region and interacts with K19, led us to address the requirement of plastin 1 for BB assembly and maintenance in a knockout mouse model. Ultrastructural analysis of the apical region of the enterocytes revealed conspicuous alterations: MV are shorter, their core actin bundles characteristically lack a true rootlet portion, and the composition of the TW is altered. Consequently, the BBs are sensitive to biochemical manipulations and degrade easily. These alterations may account for the decreased transepithelial resistance, increased cellular turnover, and the increased sensitivity to colitis induced by dextran sodium sulfate (DSS) of these mice. Plastin 1 emerges as a major scaffold of the TW region, in which it may link intermediate filaments and actin microfilaments, and as an important regulator of the morphological structure and stability of the BB and thus of intestinal physiological functions.

MATERIALS AND METHODS

Coprecipitation from Cell Lysates with Glutathione Transferase (GST)-Plastin 1

Intestinal epithelial cells were isolated as described previously (Weiser, 1973), with modifications. The lumen of freshly removed small intestine was washed with 154 mM NaCl und 1 mM dithiothreitol (DTT) and cut into three pieces. The pieces were end-ligated, and the tubes were filled with phosphate-buffered saline (PBS). The tubes were incubated in PBS for 15 min in a water bath at 37°C and then opened on one end and emptied. They were then refilled with PBS containing 1.5 mM EDTA and 0.5 mM DTT and incubated for 30 min at 37°C. The resulting suspensions were collected by gently pressing the intestine. The epithelial cells were sedimented by centrifugation ($900 \times g$ for 5 min), washed with PBS, and disrupted with a Dounce homogenizer.

Plastin 1 was expressed in *Escherichia coli* as GST fusion and coupled to glutathione-Sepharose beads (GE Healthcare, Chalfont St. Giles, Buckinghamshire, United Kingdom) by using standard methods. Intestinal epithelial cells were lysed in lysis buffer (50 mM Tris-HCl, pH 8.0, 150 mM NaCl, 20 mM $MgCl_2$, 5 mM EGTA, 1% Triton X-100, and 1% Nonidet P-40) supplemented with protease inhibitor cocktail (Sigma-Aldrich, St. Louis, MO). The cell lysate was incubated with the beads for 2 h or overnight at 4°C. After several washings with lysis buffer (eventually supplemented with 300 mM NaCl), protein complexes were eluted with SDS sample buffer. Alternatively, to maintain actin in monomeric form during the pulldown, the cells were lysed in the presence of 10 μM latrunculin A (Sigma-Aldrich), and the drug was allowed to act for 20 min before incubation with the beads. A similar procedure was used to assay coprecipitation of recombinant keratins. The GST-plastin 1–coupled glutathione-Sepharose beads were incubated with 0.09 nmol of K8 and/or K19 (Fitzgerald Industries International, Concord, CT) in a slightly different buffer (50 mM Tris-HCl, pH 8.0, 150 mM NaCl, 20 mM $MgCl_2$, 2 mM EDTA, 0.1% Triton, 1 mM phenylmethylsulfonyl fluoride [PMSF], 1 mM benzamidine, and protease inhibitor cocktail).

Generation of a Plastin 1 Knockout Mouse Strain

The mouse genomic DNA library RPCI21 from RZPD (Deutsches Resourcezentrum für Genomforschung, Berlin, Germany) was screened using Southern blot analysis with a Pls1 cDNA probe encompassing the first 430 base pairs of the coding region. Bacterial artificial chromosome (BAC) clone RPCIP711O22404Q2 was retrieved and used for further Southern blot mapping and subcloning. Targeting vector and the strategy for genotyping are depicted in Figure 2. The vector was linearized before electroporation into 129SV embryonic stem cells. Positive clones were identified by Southern blot analysis. The 5′ probe (565 base pairs) was amplified with following primers: forward (fwd), cttcatagtagggagtcatggtg; and reverse (rev), gatataattggaaaagatctaatg. The 3′ probe (1201 base pairs) was amplified with fwd, ggctacagagggcaggcaaaacc and rev, gagacactttagtgacatgaacg. A Neo probe (493 base pairs) was amplified with fwd, agggatctcctgtcatctcaccttgctcctcc and rev, gaagaactcgtcaagaaggcgatagaaggcga. An internal probe (462 base pairs) was amplified from the 3′ arm of the targeting vector using a Pls1-specific primer (gttgttgtgaactcaggtgc) and a vector-specific primer. Three clones were selected for injection into C57BL6 blastocysts. Chimeric males were then crossed with C57BL6 females to obtain heterozygous plastin 1-deficient mice. The plastin 1-deficient strain was backcrossed into C57BL6 for six generations. The following primers were used for reverse transcription-polymerase chain reaction (RT-PCR) on RNA from whole gut: E2-5′, atataaagacttgaagtagcccttccagt and E4-3′, ctgagtacgaatgctgggtgccct. Unless otherwise indicated, 8- to 12-wk-old mice were used for experiments.

Tissue Preparation and Histological Analyses

Mice were killed by cervical dislocation. The small intestine was isolated and divided in three identical parts corresponding to the duodenum, jejunum, and ileum. The large intestine was isolated near the caecum and close to the rectum. Samples were washed with ice cold PBS. For preparation of whole gut lysates, pieces of intestine were sonicated in hypotonic $NaHCO_3$ buffer (1 mM $NaHCO_3$ and 1 mM PMSF, pH 7.5). After 30-min incubation on ice, SDS buffer was added, and the samples were boiled for 10 min at 95°C, centrifuged, and the supernatants were resolved by SDS-polyacrylamide gel electrophoresis. For paraffin sectioning, short pieces of intestine were fixed in 3% paraformaldehyde (PFA), Carnoy solution (60% ethanol, 30% chloroform, 10% acetic acid), methanol or Afa (5% acetic acid, 75% ethanol, 2% formaldehyde), dehydrated in ethanol and embedded in paraffin. For cryosections, tissues were fixed for 2 h in PFA, incubated overnight in a 30% glucose solution, embedded in optimal cutting temperature media, and frozen at −80°C. Sections (5 μm) were stained with hematoxylin and eosin (HE) or processed for immunohistochemistry using standard methods. All primary antibodies used in this study are listed in Supplemental Table S1. The appropriate Alexa 488- or 568-coupled secondary antibodies were used. Nuclei were stained with propidium iodide or 4,6-diamidino-2-phenylindole (DAPI). For detection of apoptotic cells a DeadEnd fluorometric terminal deoxynucleotidyl transferase dUTP nick-end labeling (TUNEL) assay kit (Promega, Madison, WI) was used

according to the manufacturer's instructions. Images were acquired with a TCS-SP confocal laser scanning microscope (Leica, Wetzlar, Germany) or with DMR or DM 6000B conventional epifluorescence microscopes (Leica) equipped with DC 350 FX (Leica), HV-C20A (Hitachi, Tokyo, Japan), or CoolSNAP HQ (Roper Scientific, Tucson, AZ) cameras.

Isolation of Brush Borders

Two procedures were used. In the first procedure (Matsudaira and Burgess, 1979; Ferrary *et al*., 1999), the whole small intestine was washed with ice cold PBS. The mucosa from longitudinally opened segments was scraped at 4°C with a square glass coverslip, diluted in 10 volumes/mg buffer A (10 mM imidazole, 5 mM EDTA, 1 mM EGTA, pH 7.4, and 0.2 mM DTT) supplemented with protease inhibitor cocktail, and stirred at 4°C for 1 h. Mechanical cellular disruption was then achieved with 5 strokes in a Dounce homogenizer. After centrifugation (1000 × *g* for 10 min at 4°C), the pellet was washed three times with buffer A, resuspended in buffer B (75 mM KCl, 5 mM $MgCl_2$, 1 mM EGTA, and 10 mM imidazole, pH 7.4) with protease inhibitor cocktail, and mixed with a sucrose solution in buffer B to a final 40% concentration. This sample was overlaid on the same volume of 65% sucrose solution in buffer B and centrifuged at 15,000 × *g* for 30 min at 4°C. The purified BBs were recovered at the interface of the 40%:65% sucrose gradient.

In the second procedure (adapted from Mooseker and Tilney, 1975; McConnell and Tyska, 2007), the intestine was cut into three pieces and washed with ice cold saline (150 mM NaCl and 2 mM imidazole, pH 7.2). Segments were opened longitudinally, cut into small pieces (~2 cm), and stirred in a beaker containing ice-cold sucrose dissociation buffer (SDB; 200 mM sucrose, 12 mM EDTA, 19 mM KH_2PO_4, and 78 mM Na_2HPO_4) for 30 min in a cold room. The isolated enterocytes were collected by centrifugation (300 × *g* for 8 min) in SDB, resuspended in 1 volume of homogenization buffer (10 mM imidazole, pH 7.2, 4 mM EDTA, 1 mM EGTA, and 1 mM DTT, pH 7.2) supplemented with protease inhibitor cocktail, and homogenized in a blender with two 15-s bursts at high speed. The blender was rinsed with 1 volume of buffer B′ (buffer B from the first procedure supplemented with 1 mM DTT), which was pooled with the cell homogenate. The BBs were pelleted by centrifugation (1000 × *g* for 8 min), washed with buffer B′, and resuspended in the same buffer.

Brush-Border Contraction

A flow chamber was made of a polylysine-coated coverslip fixed with double-sided tape on a microscope slide. Two parallel stripes of tape were placed on opposite sides of the coverslip, leaving a 5-mm long slit on the two other sides. Isolated BBs kept on ice were injected into the slit and allowed to adhere before washing extensively with buffer B′. The flow chamber was then placed on a microscope stage, and the adherent isolated BBs were observed by differential interference contrast microscopy. Movies were recorded at one frame every 5 s for 15 min. At ~3 min of recording, buffer B′ supplemented with 200 μM ATP was injected with a pipette into the flow chamber to replace the former solution free of ATP. The movies were acquired for the remaining time without any further manipulation. The acquisitions were made with a DM 6000B epifluorescence microscope (Leica) coupled to a CoolSNAP HQ charge-coupled device camera (Roper Scientific), and driven by MetaMorph software (MDS Analytical Technologies, Toronto, ON, Canada).

Electron Microscopy

For transmission electron microscopy (TEM), small pieces of tissue (~1–2 mm) were cut open and fixed for 2 h at room temperature in 2.5% glutaraldehyde and 2% PFA in 80 mM cacodylate buffer, pH 7.2, and 0.05% $CaCl_2$. After washing with cacodylate buffer, the tissue was postfixed for 30 min at 4°C with 1% OsO_4 and 1.5% potassium ferrocyanide in cacodylate buffer and at room temperature for 1 h with 2% uranyl acetate in 40% ethanol. The samples were dehydrated in a series of graded ethanol solutions and embedded in Epon before ultrathin sectioning. For TEM on isolated BBs, samples were incubated in buffer B′ (see Isolation of Brush Borders) containing 15 mM $MgCl_2$ and let adhere for 1 h at 4°C on glass coverslips coated with polylysine. The coverslips were washed once before fixation in 0.1 M sodium phosphate buffer, pH 7.0, containing 2% glutaraldehyde and 2 mg/ml tannic acid for 1 h at 4°C. After washing in PBS, they were postfixed in 1% OsO_4 in 0.1 M phosphate buffer at pH 6.0 for 45 min and then with 0.5% uranyl acetate for 2 h. The samples were dehydrated in a series of graded ethanol solutions and then embedded in Epon before ultrathin sectioning. The observations were made with a Philips CM120 electron microscope (FEI, Eindhoven, The Netherlands). Image acquisition and measurements were made with the iTEM software (Olympus France SA, Rungis, France).

Transepithelial Resistance Measurements

Jejunum of fasted mice was isolated, washed in isotonic Ringer's solution (115 mM NaCl, 25 mM $NaHCO_3$, 1.2 mM $MgCl_2$, 1.2 mM $CaCl_2$, 2.4 mM K_2HPO_4, and 0.4 mM KH_2PO_4, pH 7.4), longitudinally opened, and mounted into a voltage-clamp system (surface, 0.15 cm^2; Titis Business Corporation, Paris, France). Tissue was bathed on each side with isotonic Ringer's solution at 37°C. The resistance (ohms·per square centimeter) was measured after a 30-min equilibration period.

In Vivo Experiments

All studies involving animals were approved by the corresponding institutional boards for experimental animal welfare. To induce colonic epithelial injury (Mashimo *et al*., 1996) DSS (mol. wt. 40,000; ICN Biomedicals, Aurora, OH) was administered in the drinking water (2.5%, wt/vol) for 13 consecutive days, and body weight was recorded. When mice reached extremis they were removed from the experiment and scored as dead. The survival curves were analyzed by Kaplan–Meier transform of probability versus days of DSS treatment. A p value of 0.05 was considered as significant. Three to five animals of each genotype and sex were killed after 8 d, and the large intestine was processed for histological analysis (HE staining). Scoring of damage and inflammation induced by DSS treatment was done in a blinded manner. Six sections, each 100 μm apart, from two or three pieces of the colon were scored according to three parameters, severity of inflammation, extent of inflammation, and crypt damage (Dieleman *et al*., 1998).

For 5-bromo-2′-deoxyuridine (BrdU) in vivo labeling, 5-bromo-2′-deoxyuridine (100 mg/kg body weight) was administered by intraperitoneal injection. Mice were killed, and the intestines were processed for histological analysis. Incorporated BrdU was visualized with an anti-BrdU antibody and the Super Sensitive Detection kit (BioGenex, San Ramon, CA) after incubation with prewarmed 2 N HCl followed by 0.2% trypsin at 37°C.

Molecular Biology and Other Methods

Standard molecular biology methods were essentially as described by Sambrook *et al*. (2001). Genomic DNA was extracted from mouse tails by a modified method of Laird *et al*., 1991. RNA was isolated from intestinal mucosa with an RNeasy kit (QIAGEN, Hilden, Germany). Radioactive labeling was performed with a Random Primed DNA labeling kit (Roche Diagnostics, Mannheim, Germany). PCR fragments were cloned into the pGEM-T Easy vector system (Promega) and sequenced. DNA sequencing was done at the service laboratory of the Center for Molecular Medicine (Cologne, Germany) by using an automated sequencer (ABI 377 Prism; PerkinElmer Life and Analytical Sciences, Boston, MA). For biochemical determinations in serum, a Cobas Integra 700 Instrument (Roche Diagnostics) was used at the Department of Clinical Chemistry of the Cologne University Hospital. Blood glucose concentration was measured with test strips on an Accutrend GCT apparatus (Roche Diagnostics). Unless indicated otherwise, statistical analysis was performed using Student's *t* test, and data are shown as mean ± SD. A p value of 0.05 was considered significant.

RESULTS

Plastin 1 Accumulates in the Terminal Web and Interacts with Keratin 19

Although actin filaments at the rootlets are bundled by villin and plastin 1, villin-deficient mice do not show alterations of the rootlets and TW (Ferrary *et al*., 1999). Therefore, we analyzed the immunolocalization of these two proteins in more detail. Although villin is homogeneously distributed in the apical pole of the enterocytes (Figure 5A and Supplemental Figure S3A), plastin 1 is enriched in the TW compared with the microvillar part, as shown by costaining with tropomyosin, and, coincidentally, β-actin (AC-74 antibody) (Figure 1A). We have observed that antibodies raised against actin, besides displaying a punctate cytoplasmic labeling, stain the TW strongly but the MV only faintly (also see Figure 5A), probably because the densely packed microvillar actin is not as easily accessible to antibodies as in the rootlets. We thus hypothesized that apart from its role as an actin-bundling protein, plastin 1 may play a specific role in the TW and perhaps establish links to components of the apical cytoskeleton other than actin filaments. We performed pulldown experiments on epithelial cell lysates by using GST-fused recombinant plastin 1 (Figure 1B) under conditions of high ionic strength (300 mM NaCl) or in the presence of 10 μM latrunculin A, which provokes depolymerization of F-actin, to rule out any possible cosedimentation being bridged by actin filaments. We found that neither condition resulted in the association of actin to the GST-plastin 1–loaded beads. We then used a panel of antibodies recognizing BB components to probe the eluates in Western

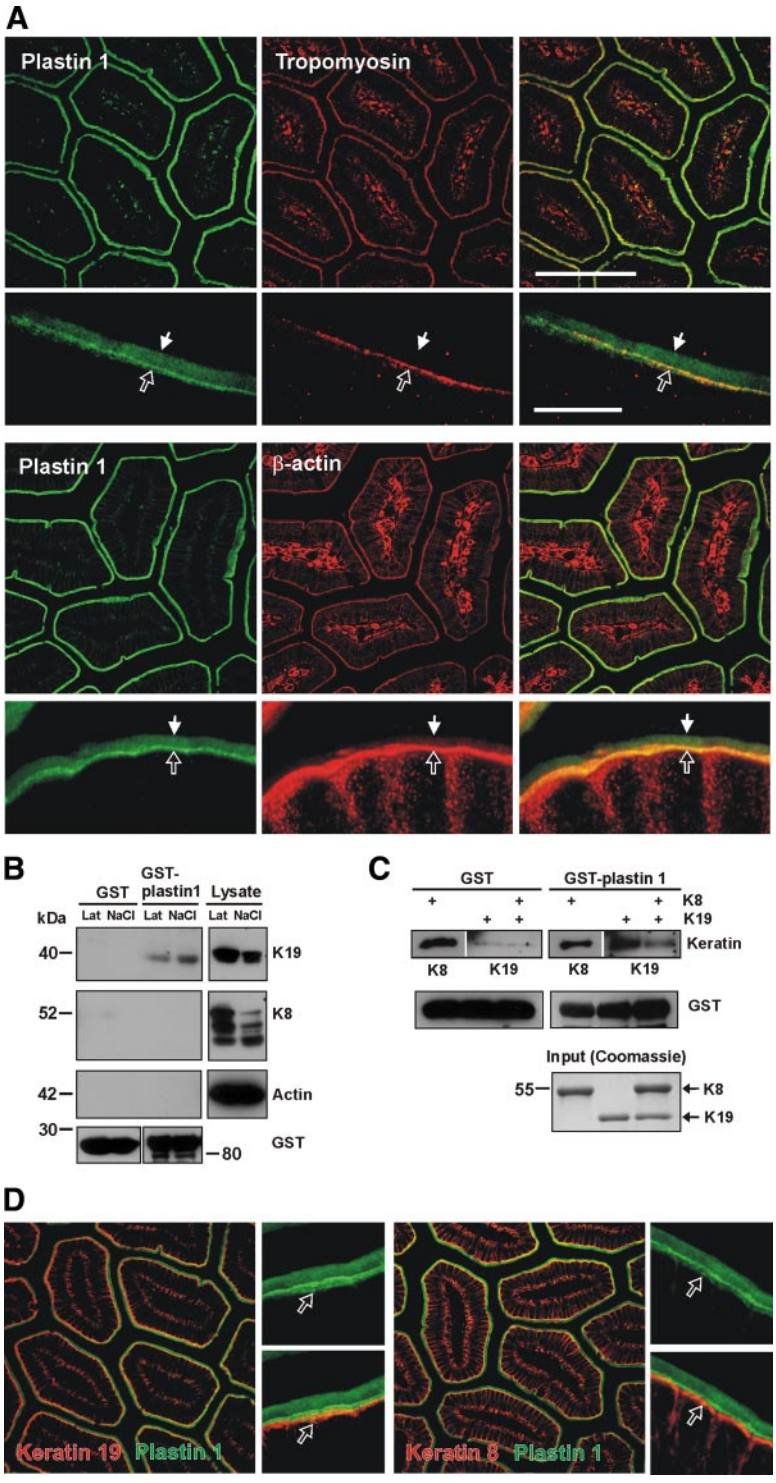

Figure 1. Plastin 1 accumulates in the terminal web and interacts with keratin 19. (A) Enrichment of plastin 1 in the TW. Paraffin sections of jejunum were incubated with primary antibodies against the indicated proteins. In the high-magnification panels, white arrows mark the position of the MV tip and black arrows the position of the TW, in which tropomyosin is mainly localized and β-actin (stained with antibody AC-74) strongly immunostains. Images were acquired with a confocal laser scanning microscope and overlaid. Bars, 100 μm for the overview panels and 15 μm for the high-magnification panels. (B) GST-plastin 1 and GST were immobilized on glutathione-Sepharose and incubated with epithelial cell lysate in the presence of 10 μM latrunculin A in low salt (150 mM NaCl) buffer (indicated by Lat) or in the absence of latrunculin A in high salt (300 mM NaCl) buffer (indicated by NaCl). Protein complexes were resolved by SDS-PAGE, blotted onto nitrocellulose, and probed with antibodies against K8, K19, actin, and GST. (C) A pulldown was performed with GST-plastin and GST and recombinant keratins as indicated. Protein complexes were processed as in B. Note that with this approach, K8 binds unspecifically to GST or to the glutathione agarose beads, yielding inconclusive results. (D) Partial colocalization of plastin 1 with the keratin network. Paraffin sections of jejunum were incubated with primary antibodies against the indicated proteins. In the high-magnification panels, black arrows mark the position of the keratin network. Magnifications as in A.

blots and found a positive signal only for K19 but not for K8. To check whether this interaction is direct, we used a similar approach with recombinant keratins. As for the pulldowns on cell lysates, purified K19 cosedimented with plastin 1–loaded beads (Figure 1C). Under the same conditions, K8 was observed to bind unspecifically to the beads or to GST, yielding inconclusive results for this keratin. We can thus conclude that plastin 1 and K19 interact directly. These experiments indicate that plastin 1 could establish a direct link to the keratin network, with which it partially colocalizes in the TW region (Figure 1D).

Plastin-deficient Mice Show No Overt Phenotype

To investigate the role of plastin 1, we designed a targeting vector in which exon 2 of the *Pls1* locus was replaced by a neomycin resistance cassette (Figure 2). Immunoblot and immunostaining analysis of intestine samples ruled out any compensation of the plastin 1 deficiency by plastin 2 or 3

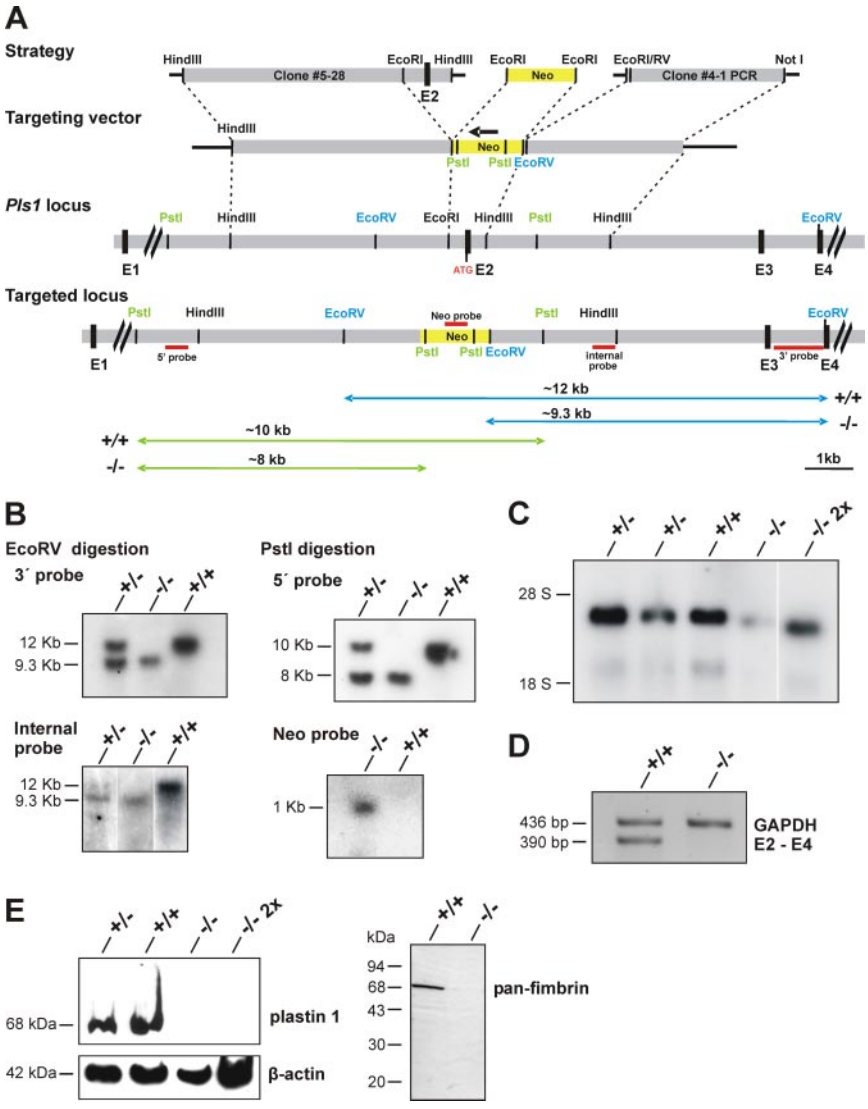

Figure 2. Generation of a plastin 1-deficient mouse strain. (A) Targeting vector. A neomycin resistance cassette replaces the second exon of the plastin 1 gene (*Pls1* locus), which contains the start codon. The 5′ and 3′ arms of the targeting vector were subcloned from BAC clone RPCIP711O22404Q2. The 5′ arm (5.5 kb) was a HindIII subclone in pBluescript from which an EcoRI fragment was excised to remove exon 2. The 3′ arm (3.4 kb) was initially a HindIII subclone used as a template for PCR amplification with engineered restriction sites for subsequent cloning into the vector containing the 5′ arm as an EcoRI-NotI fragment. An EcoRV restriction site was engineered immediately after the EcoRI site to facilitate genotyping. The neomycin resistance cassette was inserted in the EcoRI site between both genomic DNA arms. The position of the probes used for screening and genotyping is indicated (red lines); they were obtained by PCR amplification. Restriction sites used for genotyping and the expected restriction fragments are indicated in blue and green. (B) Southern blot analysis. Genomic DNA from tail biopsies was cut with the indicated restriction enzymes, resolved in agarose gels and blotted onto nylon membranes. The position of the probes and the expected sizes of the respective restriction fragments are shown in A. (C) Northern blot analysis. Total RNA (10 μg) from intestinal mucosa was resolved in denaturing agarose gels and blotted onto nylon membranes. One lane was loaded with double amount of RNA. The membrane was probed with radioactively labeled plastin 1 cDNA. The *Pls1*$^{-/-}$ mouse expresses low amounts of a plastin 1 mRNA of slightly smaller size. (D) The plastin 1 transcript of the *Pls1*$^{-/-}$ mouse lacks exon 2. Standard RT-PCR was performed with 1–5 μg of RNA isolated from whole gut using E2-5′ and E4-3′ primers. Glyceraldehyde-3-phosphate dehydrogenase (GAPDH) primers were used as control. (E) Western blot analysis of small intestine lysates. Samples were resolved by SDS-PAGE, blotted onto nitrocellulose, and probed with the indicated antibodies followed by enhanced chemiluminescence detection. One lane was loaded with double amount of lysate. No plastin 1 is detectable in the lysate from the *Pls1*$^{-/-}$ mouse. β-Actin was used as loading control. The transcript observed on the Northern blot (C) is probably unstable and not translated. To rule out that truncated species of plastin 1 are expressed in the *Pls1*$^{-/-}$ mouse we used a pan-fimbrin polyclonal antiserum that recognizes epitopes all along the protein (and can therefore detect all three plastin isoforms). No shorter plastin 1 species were observed (right).

(Supplemental Figure S1). Plastin 1-deficient mice are fertile and display a normal reproductive rate. Sex distribution of pups, inheritance of the recombined allele, and life span were not significantly changed. No alterations in body size and weight are apparent in *Pls1*$^{-/-}$ versus *Pls1*$^{+/+}$ mice (Supplemental Figure S2A), and no obvious differences in behavior have been observed. We determined the serum concentration of several metabolic parameters that depend on intestinal absorption, such as glucose, cholesterol, and triglycerides. Because plastin 1 is also expressed in the kidney, creatinine levels were also determined. None of these parameters changed in the *Pls1*$^{-/-}$ mice (Supplemental Table S2). The lack of metabolic defects linked to potential intestinal absorption alterations in the *Pls1*$^{-/-}$ mice could be because of compensation by increased food intake, decreased stool production, or increased length of the intestine (Supplemental Figure S2, B and C). However, these were not significantly different in the *Pls1*$^{-/-}$ versus *Pls1*$^{+/+}$ animals.

To investigate whether plastin 1 deficiency results in morphological alterations of the intestinal epithelium, we analyzed HE-stained sections of all intestinal segments. No obvious changes in the organization of villi or crypts were observed in the *Pls1*$^{-/-}$ mice (Supplemental Figure S2D). The distribution of the major cell types (absorptive and goblet cells) of the intestinal epithelium was also unaltered (unpublished data).

In the Absence of Plastin 1, Microvilli Are Shorter and Lack Rootlets

To study the ultrastructure of the apical pole of enterocytes in *Pls1*$^{-/-}$ animals, we performed TEM analysis of intestine sections. The enterocytes of *Pls1*$^{-/-}$ animals present the characteristic apico-basal polarity and clearly develop apical MV (Figure 3A). At higher magnification, the striated pattern of actin filaments is observed in MV of both *Pls1*$^{+/+}$ and *Pls1*$^{-/-}$ mice (Figure 3B). However, in *Pls1*$^{+/+}$ sections, the

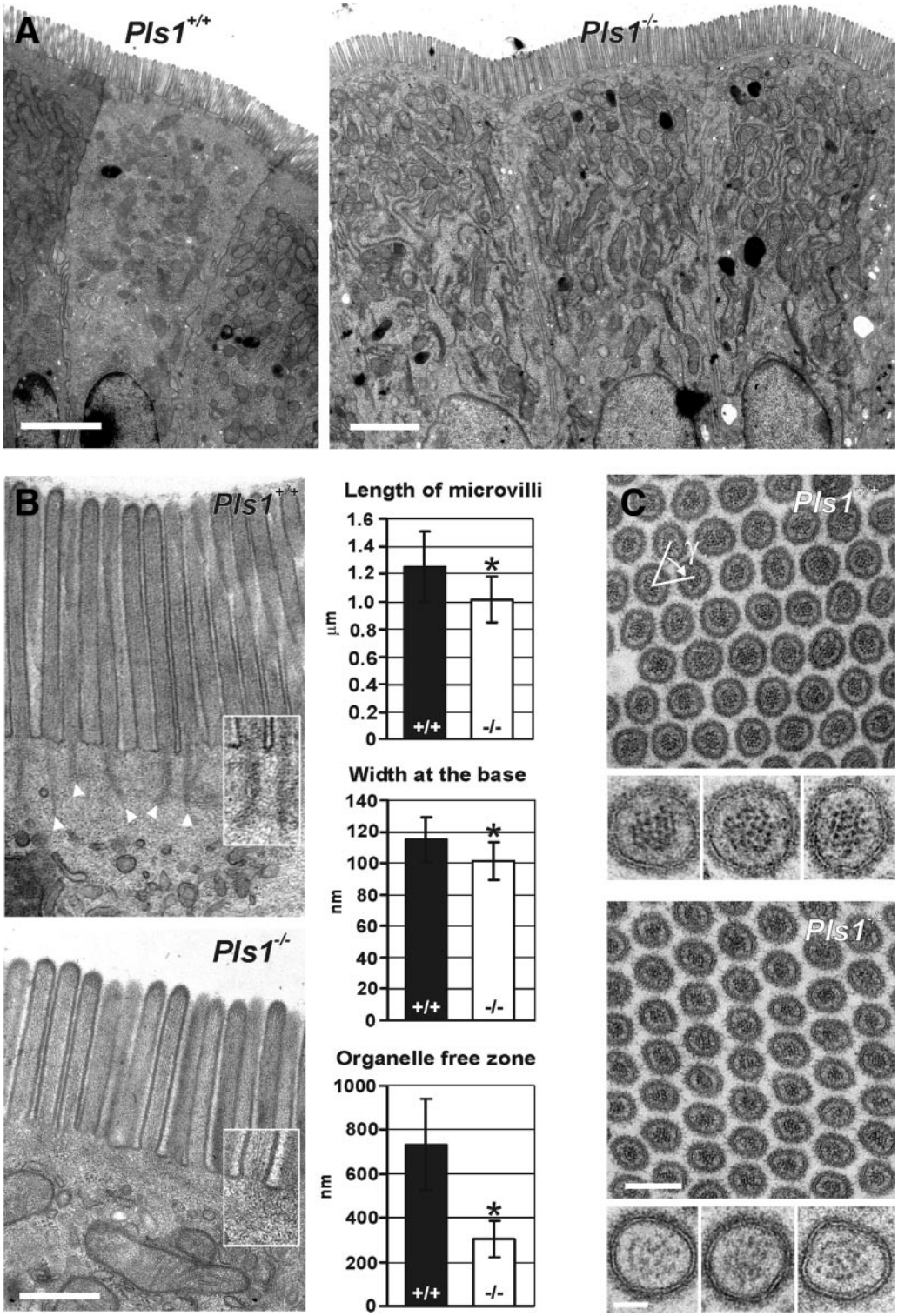

Figure 3. Microvilli are present in the absence of plastin 1, but they are shorter and devoid of rootlets. Sections of jejunum of *Pls1*$^{+/+}$ and *Pls1*$^{-/-}$ mice were analyzed by transmission electron microscopy. (A) At low magnification, the enterocytes from *Pls1*$^{-/-}$ mice present the expected polarity and develop apical MV. Bars, 2 μm. (B) The morphology of MV was analyzed at higher magnification of sections cutting the MV longitudinally. In the *Pls1*$^{-/-}$ mouse, the MV are shorter, and their base is constricted. The organelle free zone of the TW is narrowed. Rootlets are clearly absent as highlighted in the insets at higher magnification (1.5×). The end of each rootlet is indicated in the *Pls1*$^{+/+}$ section by a white arrowhead. Values are mean ± SD, *p $<$ 0.0001, Student's *t* test. Bar, 500 nm. (C) Cross sections of MV show their reticular organization. The density of the MV was not altered. The angle γ formed by three adjacent MV is not significantly different between *Pls1*$^{-/-}$ and *Pls1*$^{+/+}$ sections and is approximately the expected 60°. Bar, 200 nm. Examples of individual MV at high magnification are shown underneath the corresponding panel. Note the lower contrast of the core bundle in the *Pls1*$^{-/-}$ section, probably reflecting an altered organization. Bar, 50 nm.

rootlets are easily detected as elongated electron dense structures, whereas they are never observable with this technique in *Pls1*$^{-/-}$ samples (Figure 3B, insets). Moreover, *Pls1*$^{-/-}$ MV are 20% shorter than their *Pls1*$^{+/+}$ counterparts (1.25 ± 0.26 μm, n = 86 in *Pls1*$^{+/+}$and 1.01 ± 0.16 μm, n = 194 in *Pls1*$^{-/-}$; $p < 0.0001$) and show a slight basal constriction (width at the base, 115 ± 14.5 nm, n = 142 in *Pls1*$^{+/+}$and 101.3 ± 11.9 nm, n = 164 in *Pls1*$^{-/-}$; $p < 0.0001$) (Figure 3B). Finally, in *Pls1*$^{+/+}$ mice, organelles are excluded from the very apical part of the cytoplasm corresponding to the TW region. In *Pls1*$^{-/-}$ mice, this zone of organelle exclusion is strongly narrowed to ~40% of its width in *Pls1*$^{+/+}$ samples (731.4 ± 206.5 nm, n = 17 in *Pls1*$^{+/+}$ and 304.9 ± 83.8 nm, n = 26 in *Pls1*$^{-/-}$; $p < 0.0001$) (Figure 3B). To analyze their degree of organization, we measured diameter, perimeter, area, and density of transversal sections through the MV, which did not differ significantly (unpublished data). The packing angle γ formed by three adjacent MV, which is expected to be of 60° for tightly packed perfect cylinders, was not modified in the absence of plastin 1 (65.9 ± 9.7°, n = 115 in *Pls1*$^{+/+}$; 62.0 ± 12.1°, n = 89 in *Pls1*$^{-/-}$) (Figure 2C). We were not able to accurately evaluate the number of actin filaments per microvillus in the *Pls1*$^{-/-}$ sections because the quality and contrast of the dotted filament pattern is poor compared with the *Pls1*$^{+/+}$ counterparts (Figure 3C, sections at higher magnification). Presumably, this reflects a different organization of the actin bundles in the absence of plastin 1.

Brush Borders of Plastin 1-deficient Mice Are Highly Fragile

As indicated by the striated (Figure 3B) or punctate (Figure 3C) patterns observed, respectively, in longitudinal and transversal TEM sections, actin filaments are still present in *Pls1*$^{-/-}$ MV. To better understand the organization of the actin cytoskeleton inside MV, we performed TEM on isolated BBs. This technique preserves the plasma membrane and the cytoskeleton of the apical pole and washes out the soluble components, greatly increasing the contrast and allowing the observation of individual actin filaments. The first isolation procedure we used (Matsudaira and Burgess, 1979; Ferrary *et al*., 1999) gave very good results for the *Pls1*$^{+/+}$ BBs, whereas only a very few damaged BBs were obtained from the *Pls1*$^{-/-}$ mouse intestine (Figure 4A). We modified this method by using an F-actin–stabilizing buffer (Mooseker and Tilney, 1975; McConnell and Tyska, 2007). This greatly increased the stability of the *Pls1*$^{-/-}$ BBs, which were nicely preserved and obtained with a similar yield as *Pls1*$^{+/+}$ BBs (Figure 4B). Phalloidin labeling confirmed the preservation of the actin cytoskeleton in both samples (Figure 4B, insets). This preparation was used for TEM, where F-actin filaments aligned in parallel array are clearly observed in both *Pls1*$^{-/-}$ and *Pls1*$^{+/+}$ samples (Figure 4C). The myosin 1 bridges between actin filaments and the plasma membrane are also detected in both preparations (Figure 4C, insets, arrowheads). The constriction at the base of the MV is clearly seen in isolated *Pls1*$^{-/-}$ BBs. The better contrast achieved by TEM on isolated BBs showed highly rudimentary rootlets composed of only few short filaments going beyond the level of the plasma membrane in *Pls1*$^{-/-}$ BBs (Figure 4C, insets). Nevertheless, these clearly differ from the long and dense rootlets observed in the *Pls1*$^{+/+}$ situation, emphasizing the previous results (Figure 3).

The Composition of the Terminal Web, but Not of the Microvilli, Is Altered in the Plastin 1-deficient Mouse

We next investigated whether the amounts and localization of microvillar components were altered as a consequence of plastin deficiency (Supplemental Figure S3A). As expected,

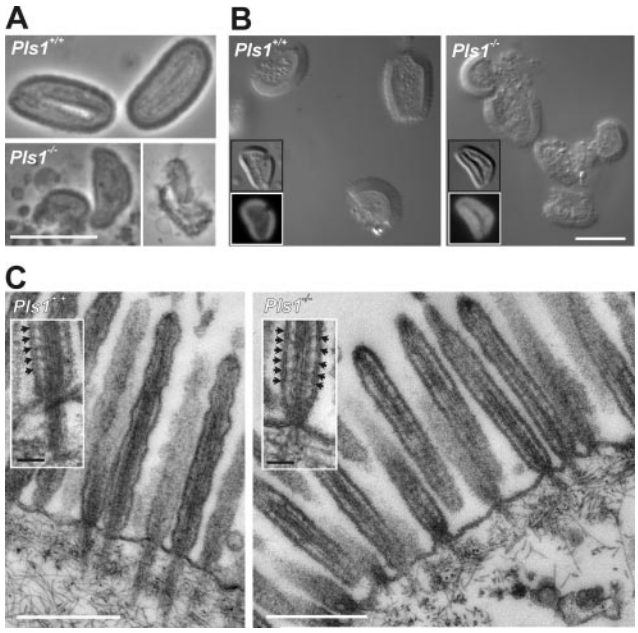

Figure 4. Brush borders are fragile in the absence of plastin 1. (A) Phase contrast images of BBs isolated with a classical procedure that uses a hypotonic buffer for the washes. *Pls1*$^{+/+}$ BBs are nicely preserved, whereas only few damaged BBs remain in the *Pls1*$^{-/-}$ preparation. Bar, 10 μm. (B) Interference contrast images of BBs isolated using an F-actin–stabilizing buffer for the washes. This method allows a good preservation of BBs from the *Pls1*$^{-/-}$ mice. Bar, 10 μm. The BBs conserve an F-actin cytoskeleton as shown by FITC-labeled phalloidin staining (insets). (C) Transmission electron microscopy on isolated BBs shows the presence of actin bundles, but rootlets are either absent or contain only few and very short filaments in the MV of *Pls1*$^{-/-}$ mice. Bars, 500 nm. The insets show higher magnification pictures to demonstrate intact myosin I bridges (arrows) and highlight the poor actin organization of the *Pls1*$^{-/-}$ rootlets compared with the *Pls1*$^{+/+}$. Bars, 100 nm.

staining of F-actin with fluorescein isothiocyanate (FITC)-phalloidin revealed no alterations in cryosections of the small intestine of *Pls1*$^{-/-}$ animals. Staining for villin and espin yielded the typical pattern of MV distribution both in *Pls1*$^{-/-}$ and *Pls1*$^{+/+}$ animals. No alterations were also found in the distribution of ezrin and two class I myosins, myosin 1a and myosin 1e, that link the actin core bundles to the plasma membrane. In addition, Western blot analysis revealed no changes in the expression levels of any of these proteins in isolated BBs, except for a slight reduction in the amount of β-actin (Figure 5B). We conclude that the absence of plastin 1 does not result in compensatory overexpression or altered distribution of other actin-binding proteins in the enterocyte MV.

The loss of the actin rootlets observed in TEM pictures (Figures 3B and 4C) prompted us to examine the TW region in more detail. Spectrin and myosin II form thin filaments that connect adjacent rootlets. Myosin II additionally associates with the actin filaments of the adhesion belt (Glenney *et al*., 1982; Hirokawa *et al*., 1982). Tropomyosins show a polarized distribution (Percival *et al*., 2000), with isoforms 5a and 5b displaying a predominantly apical localization (Dalby-Payne *et al*., 2003). They stabilize the microfilaments of the actin core only at the rootlets and are not found within the MV (Bretscher and Weber, 1978). Loss of plastin 1 leads to major alterations in the localization of these proteins (Figure 5A). Stainings for α-II-spectrin and myosin IIa

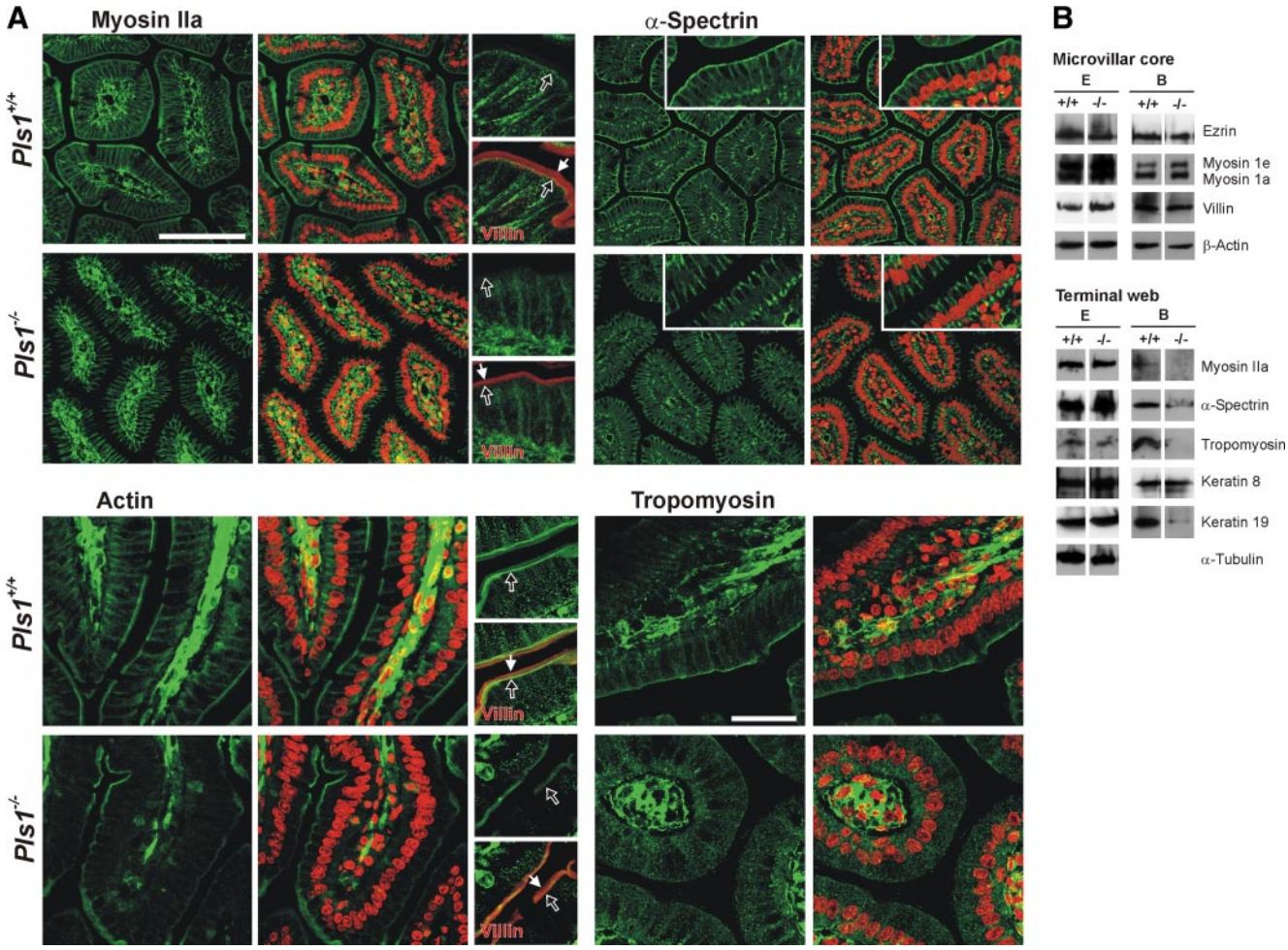

Figure 5. Alterations in the terminal web in the plastin 1-deficient mouse. (A) Paraffin sections of jejunum were incubated with primary antibodies against the indicated proteins. Insets and small panels show regions at higher magnification. Nuclei were stained with propidium iodide and are shown in red in the merged pictures. A double staining with villin (in red in the enlarged myosin IIa and actin panels) shows that MV are intact. Images were acquired with a confocal laser scanning microscope. White arrows mark the position of the MV tip, black arrows the position of the TW region. In the *Pls1*$^{-/-}$ mouse, myosin II and spectrin are absent from the TW but still present along the basolateral membranes. Some actin staining remains in the MV, but the TW signal is absent. Tropomyosin staining is weaker in the TW region. Bars, 30 μm for actin and tropomyosin and 100 μm for the others. (B) Western blot analysis of BB components. Lysates (equal amounts of total protein) of intestinal epithelial cells (labeled E) or isolated brush borders (labeled B) were resolved by SDS-PAGE, transferred onto nitrocellulose, and membranes were probed with antibodies against the indicated proteins. Tubulin was used as a loading control for epithelial cells. Although microvillar components are essentially unaltered in BB lysates, the amounts of most TW components are strongly reduced.

showed that neither of them localizes to the TW in *Pls1*$^{-/-}$ mice, whereas their basolateral localization is not affected. Staining for tropomyosin revealed a strongly decreased signal in the TW region of the *Pls1*$^{-/-}$ mice. In contrast to the unaltered F-actin staining observed with phalloidin (Supplemental Figure S3A), we found an altered localization pattern with three different antibodies against actin: two antibodies (AC-74 and a polyclonal antibody) specific for β-actin and the wide-spectrum anti-actin antibody AC-40. Although in the *Pls1*$^{-/-}$ mouse the TW staining was lost, the fainter microvillar and the punctate cytoplasmic distributions were unaffected. The decreased actin staining in the TW of the *Pls1*$^{-/-}$ sections is thus consistent with the lack of rootlets.

Because the TW region is connected to the underlying intermediate filament and microtubule networks and because plastin 1 is able to bind K19, we also examined those in intestinal sections. No alterations were found in the subcellular distribution of either α- or γ-tubulin or of the keratin network as assessed with a pancytokeratin antibody (Supplemental Figure S3B). Specific stainings for K8 and K19 did not reveal noticeable changes in their respective distribution patterns in the enterocytes of *Pls1*$^{-/-}$ mice (Supplemental Figure S3C). Finally, Western blot analysis on lysates of whole epithelial cells did not reveal alterations in the amounts of any of the components mentioned above. However, consistent with the immunohistochemistry data, dramatically reduced levels of myosin IIa, α-II-spectrin, and tropomyosin 5a/5b were observed in isolated BBs from *Pls1*$^{-/-}$ mice. Notably, although the amount of K8 was unaffected, the amount of K19 associated to BBs was substantially reduced in *Pls1*$^{-/-}$ samples (Figure 5B).

In view of these strong TW defects, in particular of myosin II redistribution, we challenged the functionality of the actomyosin networks of the BBs by performing ATP stimulation assays. The stimulation of isolated BBs by ATP provokes the contraction of the TW region and the shedding of membrane at MV tips (McConnell and Tyska, 2007). The first effect is because of the contraction of the actin/myosin II belt

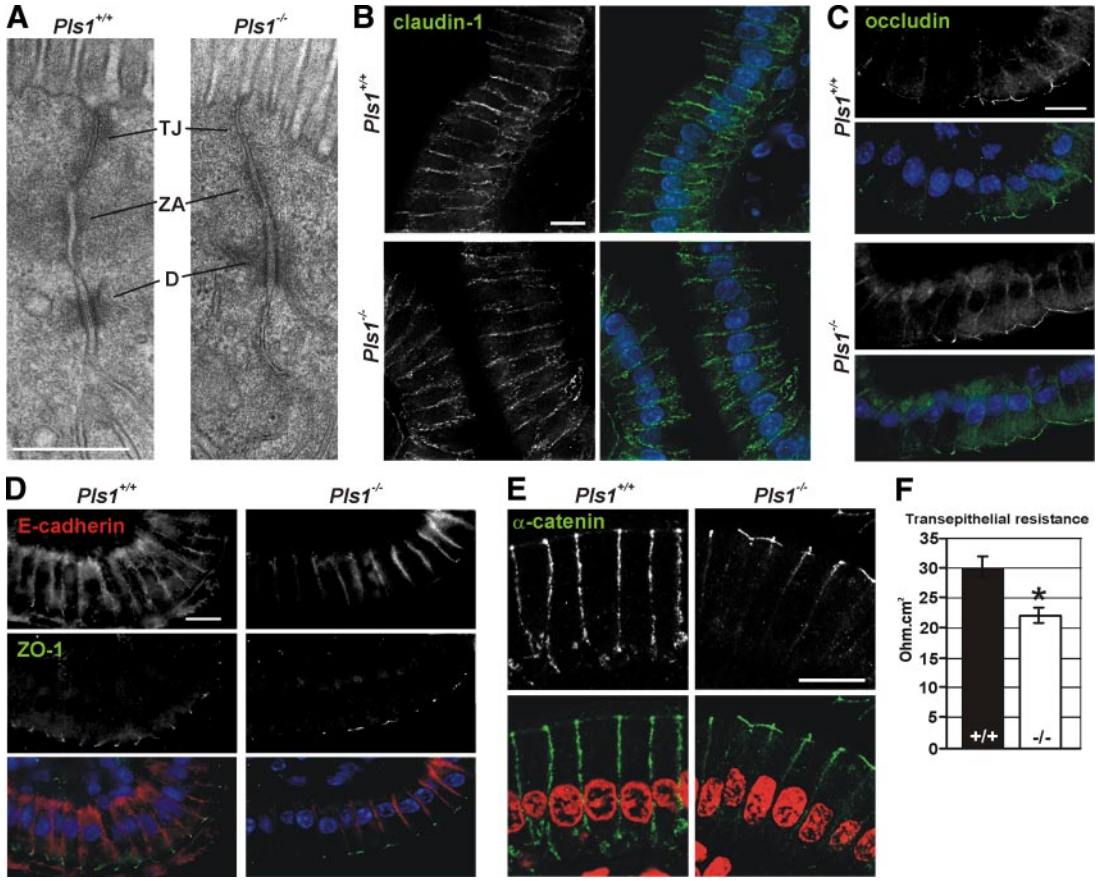

Figure 6. Morphology and functionality of the junctional complexes in the plastin 1-deficient mouse. (A) Transmission electron micrographs of the junctional complex of intestinal epithelial cells from $Pls1^{+/+}$ and $Pls1^{-/-}$ mice. TA, tight junction; ZA, zonula adherens; and D, desmosome. Bar, 500 nm. (A–E) Paraffin sections of jejunum were incubated with primary antibodies against claudin-1 (B), occludin (C), E-cadherin and ZO-1 (D), and α-catenin (E). Nuclei were stained with DAPI (B–D) or propidium iodide (E) and are shown in blue or red, respectively, in the merged pictures. None of these proteins are affected in the $Pls1^{-/-}$ mice. Images were acquired with a confocal laser scanning microscope. Bars, 10 μm. (F) Transepithelial resistance of the jejunal epithelium. Samples were assayed in a Ussing chamber. A significant reduction is observed in the $Pls1^{-/-}$ samples. Values are mean $\pm$ SD. *$p < 0.05$, Student's t test.

linked to adherens junctions and the membrane shedding is the consequence of myosin 1a movement toward the plus ends of the actin bundles. These effects were, however, preserved in the $Pls1^{-/-}$ BBs (data not shown), and the contraction could be inhibited in $Pls1^{-/-}$ and $Pls1^{+/+}$ samples by the addition of the myosin II inhibitor blebbistatin. This striking result in view of the strong delocalization of myosin II can be explained by the fact that only a tiny pool of the TW myosin II is required for BB contraction (Keller *et al.*, 1985). This is consistent with myosin II being present all along the lateral surface of the $Pls1^{-/-}$ enterocytes up to the adhesion belt (Figure 5A).

The Transepithelial Resistance Is Reduced in Plastin 1-deficient Mice but the Structure of the Junctional Complexes Is Apparently Preserved

Because the TW is linked to the junctional complex that seals the intestinal epithelium, we investigated whether the alterations observed in the TW of the $Pls1^{-/-}$ mice have any impact on the morphology of this complex. No noticeable morphological changes in the junctional complex were observed in transmission electron micrographs of $Pls1^{-/-}$ sections (Figure 6A). Stainings for the transmembrane elements of the tight junctions claudin-1 and occludin (Figure 6, B and C) or for the zonula occludens 1 (ZO-1) protein that connects the tight junctions with the actin cytoskeleton (Figure 6D) did not reveal any alteration in the $Pls1^{-/-}$ mouse. Similarly, no alterations were noticed in the localization of the transmembrane component of the adherens junctions E-cadherin (Figure 6D) or of the proteins that link the adherens junction to the actin belt, α-catenin (Figure 6E) and β-catenin (data not shown). The absence of noticeable morphological alterations does not rule out a difference in functionality. Indeed, measurements of the transepithelial resistance showed a significantly reduced resistance in the jejunum of $Pls1^{-/-}$ (21.93 $\pm$ 2.03 ohm cm^2, n = 6) compared with $Pls1^{+/+}$ mice (29.90 $\pm$ 2.70 ohm cm^2, n = 7; $p < 0.05$) (Figure 6F).

Plastin 1-deficient Mice Are Sensitive to DSS-induced Colitis

The observations of the fragility of the isolated BBs and the decreased transepithelial resistance of $Pls1^{-/-}$ mice prompted us to investigate the stability of the intestinal epithelium by using a model of colitis induced by DSS, an agent that causes mild epithelial injury when administered orally (Mashimo *et al.*, 1996). In general, $Pls1^{-/-}$ mice seemed more sensitive to the effects of DSS. $Pls1^{-/-}$ animals of both sexes exhibited evidence of a colitis, with anal bleeding or prolapse occurring at day 5, whereas in $Pls1^{+/+}$ animals symptoms were apparent 2 d later. $Pls1^{-/-}$ females were significantly more sensitive,

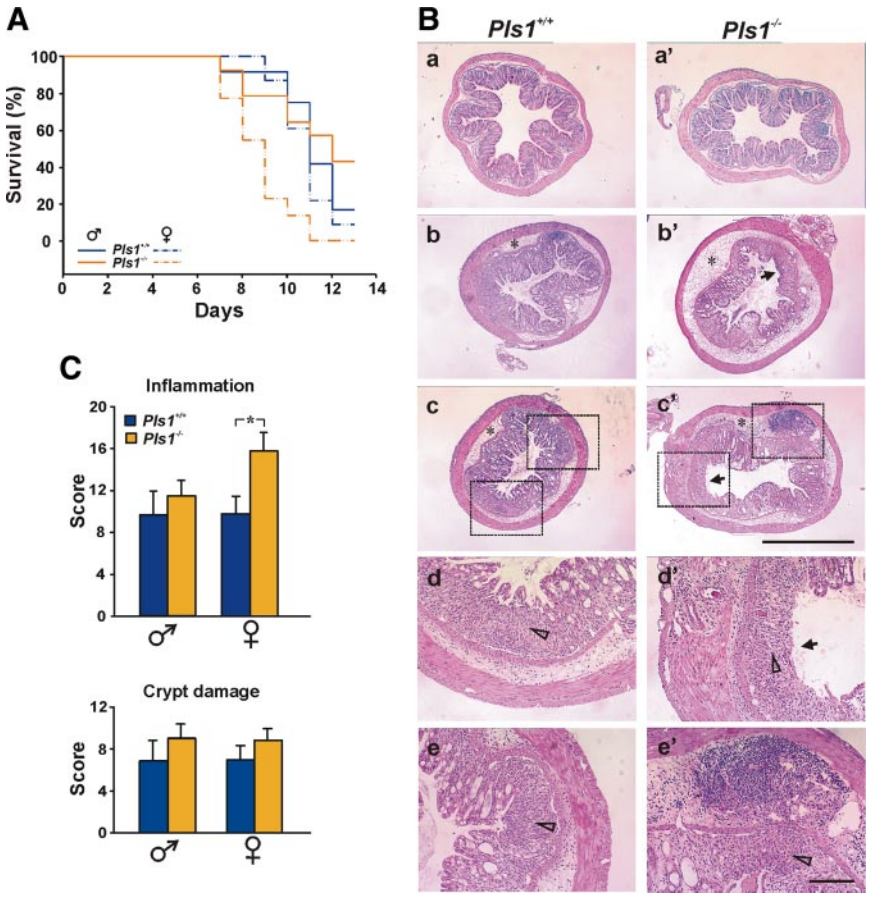

Figure 7. Increased sensitivity to DSS-induced colitis in the plastin 1 deficient mouse. (A) Survival graph. Colonic epithelial injury was induced with 2.5% DSS in the drinking water for 13 consecutive days. Data are cumulative of two independent experiments, with a total of 12–23 mice for each population. Female $Pls1^{-/-}$ mice died significantly earlier than $Pls1^{+/+}$ ($p < 0.0001$, log rank, Kaplan–Meier transform). (B) Histological analysis of DSS induced damage. Three to five animals of each genotype and sex were killed after 8 d of DSS treatment. Samples from the central part of the colon were processed for histological analysis (HE staining). Shown are representative sections from untreated animals (a, a′), treated males (b, b′), and treated females (c, c′) as well as higher magnification details (d, e; d′, e′) of the c and c′ sections as indicated. Asterisks indicate distension of the submucosa caused by edema. White arrowheads show leukocyte infiltration of the mucosa and destruction of the crypt morphology. Black arrows mark lesions with complete loss of the epithelium. In f′, a large submucosal abscess is shown at high magnification. Bars, 1 mm for the low-magnification sections, 150 μm for the high-magnification sections. (C) Scoring of DSS induced lesions. HE stained sections from three to five animals of each genotype and sex were assigned a score according to severity and extent of inflammation and crypt damage (see *Materials and Methods*). Data are mean ± SEM. Female $Pls1^{-/-}$ mice showed a significantly more severe inflammatory response to DSS.

with a 50% survival rate at 9 d (log rank, $p < 0.0001$) compared with 12 d for $Pls1^{+/+}$ females (Figure 7A). Survival rates of $Pls1^{-/-}$ males were not significantly different from those of $Pls1^{+/+}$ males, despite their earlier onset of symptoms. Inspection of the intestine after 8 d of treatment revealed in all cases ulcerations and bleeding confined to the large intestine.

Histological examination of the colon showed lesions of variable severity, with inflammatory cell infiltrates in the mucosa, destruction of the crypt morphology (Figure 7B, empty arrowheads), loss of the epithelium (Figure 7B, arrows), and distension of the submucosa (Figure 7B, asterisks) in both strains. Abscesses in the submucosa (Figure 7B, e′) were more frequent in $Pls1^{-/-}$ females than in the other populations. When severity and extension of inflammation were scored, we observed a significantly greater response in the $Pls1^{-/-}$ than in the $Pls1^{+/+}$ females (15.8 ± 1.7 vs. 9.8 ± 1.6; $p < 0.0428$), whereas males behaved similarly (11.4 ± 1.5 in $Pls1^{-/-}$ vs. 9.6 ± 2.2 in $Pls1^{+/+}$) (Figure 7C). Although we observed a trend toward higher scores of crypt damage in $Pls1^{-/-}$ mice of both sexes, the differences were not statistically significant.

Increased Epithelium Renewal in the Intestine of Plastin 1-deficient Mice

The increased fragility of the BBs and the higher susceptibility to induced colitis are in contrast to the mild phenotype displayed by the $Pls1^{-/-}$ mice. The question thus arises whether an increased epithelium renewal rate compensates for the plastin 1 deficiency. Newly generated cells in the crypts migrate toward the top of the villi within 2 to 7 d and then they undergo apoptosis and are finally shed into the lumen (Crosnier *et al*., 2006). We used a TUNEL assay to examine whether the loss of plastin 1 results in an increased apoptosis rate in the intestinal epithelium. Although occasional apoptotic enterocytes were observed in the $Pls1^{+/+}$ mice, the number of TUNEL-positive epithelial cells was increased fourfold in the $Pls1^{-/-}$ mice ($p < 0.0001$) (Figure 8, A and B). To analyze whether the increased cell loss is balanced by an increased proliferation rate, we stained the proliferation zone in the crypts for Ki67, a nuclear protein expressed during all active phases of the cell cycle, and for phosphohistone 3, a marker of cells in M phase of the cell cycle. These stainings revealed no alterations in the position and width of the proliferating zone in the $Pls1^{-/-}$ mouse (Supplemental Figure S4). A potential increase in cell renewal in $Pls1^{-/-}$ mice was analyzed in a BrdU incorporation assay (Figure 8, C and D). Two hours after BrdU administration, proliferating cells within the crypts showed a pattern similar to Ki67 staining in both $Pls1^{+/+}$ and $Pls1^{-/-}$ mice. However, after 24 h, epithelial cells of $Pls1^{-/-}$ mice occupied 52.8% of the villus length compared with 36.8% in $Pls1^{+/+}$ ($p < 0.0001$). Similarly, whereas BrdU-positive cells had nearly reached the villus tip of $Pls1^{-/-}$ mice (91.2% migration distance) at 48 h, the distance migrated by $Pls1^{+/+}$ cells was only 79.2% ($p < 0.0001$). The increased cell migration had no effect on epithelial cell differentiation, as shown by staining for I-Fabp (Supplemental Figure S4).

DISCUSSION

The analysis of the $Pls1^{-/-}$ mouse revealed that plastin 1 plays an important role for the elongation of the MV and

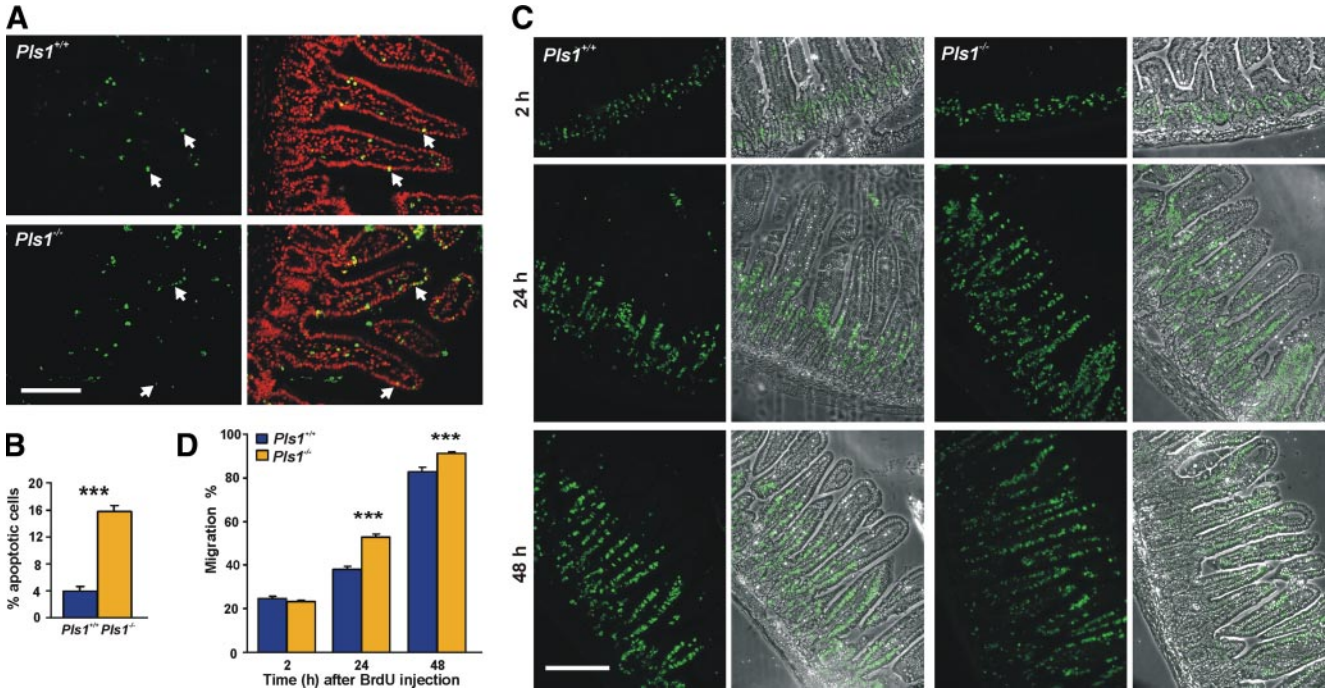

Figure 8. Increased renewal of the intestinal epithelium of plastin 1 deficient mice. (A) Apoptotic cells were detected in paraffin sections of jejunum by using a TUNEL assay. Arrows point at examples of apoptotic cells in the epithelium. Bar, 100 μm. (B) The *Pls1*$^{-/-}$ mice have a fourfold increased apoptosis rate. This was calculated as the percentage of apoptotic epithelial cell nuclei related to the total number of epithelial cell nuclei per villus section. Data are mean ± SEM of three mice, with three sections per genotype having been measured. ***$p < 0.0001$, Student's *t* test. (C) Epithelial cell migration along the villus. Mice were killed 2, 24, and 48 h after intraperitoneal injection of BrdU. Incorporated BrdU was detected on paraffin sections of jejunum after incubation with a specific antibody. Overlays with phase contrast images are also shown. Bar, 150 μm. (D) Increased migration along the villus in *Pls1*$^{-/-}$ mice. The migration rate was calculated as the distance reached by BrdU-positive cells relative to the villus length. No alterations in villus length or cell number were detected in the *Pls1*$^{-/-}$ mice. Data are mean ± SEM of three animals of each genotype per time point. Three sections of each animal were scored. ***$p < 0.0001$, Student's *t* test.

stability of the BB, although not for their de novo formation. The model we favor (Figure 9) proposes that plastin 1 contributes to anchoring the rootlets of the microvillar actin cores to the underlying keratin network. This occurs possibly through a specific interaction with K19, and loss of this anchoring would result in detached and destabilized rootlets. In the absence of plastin 1, rootlets would be unprotected and prone to faster depolymerization, and components of the TW

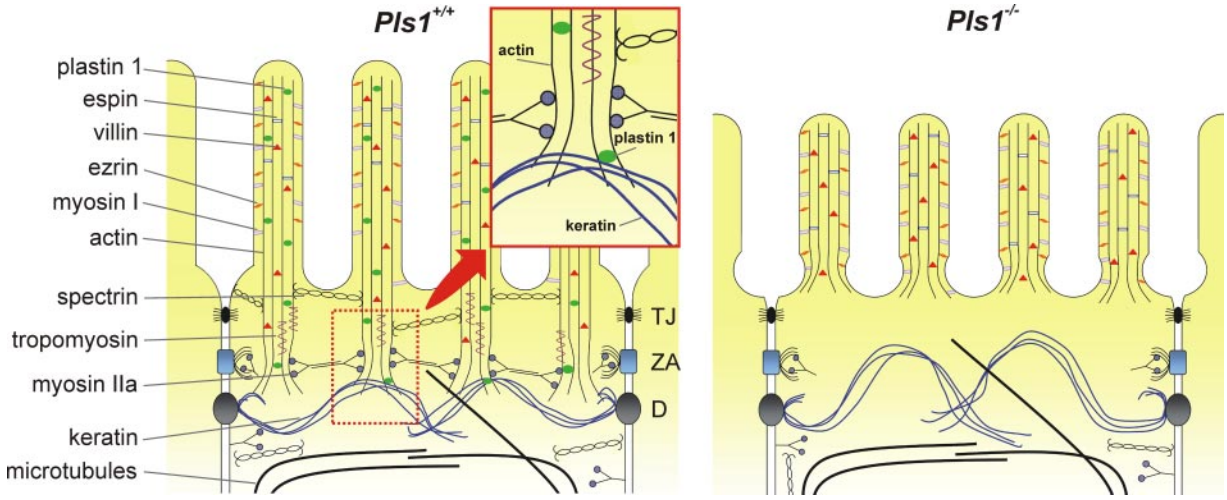

Figure 9. Model proposed to account for the consequences of the plastin 1 deficiency on the morphology of the brush border. Schematic depiction of the apical pole of the intestinal epithelial cells of *Pls1*$^{+/+}$ and *Pls1*$^{-/-}$ mice. See *Discussion* for details. The enlarged area highlights a possible role of plastin 1 as linker between the actin rootlet and the keratin network. In the *Pls1*$^{-/-}$ mouse the MV are shorter, rootlets are rudimentary or absent and the microvillar basis is narrowed. The TW is not properly assembled, resulting in a narrow organelle free region. The adhesion complexes and the microtubule and keratin networks are not noticeably affected. TJ, tight junction; ZA, zonula adherens; D, desmosome.

would no longer be recruited. Consequently, the BB would lose stability, as the microvillar actin cores are not interconnected.

Plastin 1 Is Important for Brush Border Integrity

Unlike villin, plastin 1 gives rise to actin bundles in vitro that closely resemble those of the MV core bundle (Glenney *et al*., 1981; Matsudaira *et al*., 1983). It is therefore surprising that in *Pls1*$^{-/-}$ mice MV assemble with apparently normal actin cores, although with the remarkable abnormalities discussed below. Plastin 1 deficiency is not compensated by persistent expression of either of the two other plastins that can be detected in intestinal cells and in sensory cells of the inner ear during assembly of MV and stereocilia in embryonic stages (Tilney *et al*., 1992; Daudet and Lebart, 2002). It has been proposed that villin and plastin 3 are responsible for the formation of rudimentary MV, but these reach their normal length when expression of plastin 1 starts and the protein localizes apically (Ezzell *et al*., 1989; Chafel *et al*., 1995). The existence of MV both in villin and in plastin 1 knockout mice suggests that the apical localization of plastin 3 during embryonic development could be sufficient for the formation of rudimentary MV.

However, MV also form in the adult epithelium, where plastin 3 is no longer expressed, which highlights a likely redundancy among the three actin-bundling proteins (plastin 1, villin, and espin) of the MV to warrant their morphogenesis. Villin and espin, albeit not overexpressed, must thus provide sufficient bundling activity, although TEM sections across MV suggest that the organization of the bundles is altered in the absence of plastin 1. In vitro studies assigned an essential role to villin for MV assembly (Friederich *et al*., 1990; Friederich *et al*., 1992; Costa de Beauregard *et al*., 1995); however, no alterations in the morphology and composition of the MV were found in villin deficient mice (Pinson *et al*., 1998; Ferrary *et al*., 1999; Athman *et al*., 2002). Espin-deficient mice have no apparent morphological alterations in the intestinal epithelial cells (Revenu and Robine, unpublished), presumably reflecting its low abundance relative to plastin 1 and villin.

This leaves plastin 1 as the only actin-bundling protein that by itself plays an important role for the proper formation and maintenance of intestinal MV. Our data are in agreement with the proposal that plastin 1 stabilizes and elongates existing MV but is not required for their de novo assembly (Arpin *et al*., 1994). Plastin 1 accumulates in the TW region of the BB and constitutes the first BB protein for which a deficiency results in dramatic alterations in that region, as demonstrated by the absence or reduced amount of typical components such myosin II, spectrin, and tropomyosin. This points at a general alteration that presumably results from the missing or rudimentary rootlets observed in TEM images, because these components stabilize or interconnect the rootlets, or link them to the adhesion complex (Figure 9).

Plastin 1, a Likely Linker between the Microvillar Actin and the Apical Keratin Network and a Key Factor Stabilizing the Microvillar Rootlet

That absence of plastin 1 results in clear alterations of the TW indicates that this protein fulfills a specific function that cannot be compensated by other BB proteins. The biochemical interaction of plastin 1 with the keratin network might well be at the base of the ultrastructural and functional defects observed in the BB of the *Pls1*$^{-/-}$ mice. Early TEM studies on intestinal epithelial cells showed that the intermediate filament network is linked to the microfilament network (Hirokawa *et al*., 1982, 1983). We hypothesize that plastin 1 is responsible for anchoring the rootlets to the underlying keratin network through an interaction with K19, perhaps contributing to the mechanical strength of the apical pole. Additionally, plastin 1 could have a stabilizing function for the filaments solely because of its bundling activity, as has been proposed for all bundlers from biological and biophysical studies (Zigmond *et al*., 1992; Tilney *et al*., 2003) because depolymerization beyond a cross-link requires the unbinding of the cross-linking protein (Prost *et al*., 2007). Moreover, plastin 1 could contribute to stabilizing the rootlets by preventing the action of the severing and depolymerizing protein cofilin. Such mechanism has been described for plastin 3 (Giganti *et al*., 2005) and for yeast fimbrin (Nakano *et al*., 2001) and is therefore likely to work for other plastins. It is also possible that absence of plastin 1 results in the destabilization of the rootlets indirectly through the mislocalization of tropomyosin, a protein that stabilizes actin filaments directly by slowing depolymerization from the pointed end (Broschat *et al*., 1989). The absence of plastin 1 would result in detached and unprotected rootlets, leading to the faster depolymerization of actin filaments up to the region where the actin core is attached to the plasma membrane. Consequently, the underlying keratin network becomes displaced apically, leading to a narrowed organelle free zone underneath the MV (Figure 9).

That absence of plastin 1 causes no obvious defects in the keratin network, at least with the resolution that can be achieved with the optical microscope, is not surprising. Studies in Caco2 cells have shown that the polarity of the keratin network establishes 2 d before that of the microtubules and actin filaments and the formation of the BB (Wald *et al*., 2005), therefore independently of plastin 1. The reverse, however, may not hold true. Although K19 knockout mice do not present any overt phenotype, presumably because the defects are compensated by other class I keratins, no studies have been published addressing specifically the intestinal epithelium (Tamai *et al*., 2000). Interestingly, silencing of the K19 gene in Caco2 cells results in alterations of the apical actin network that are apparently not compensated by K18 or another keratin (Salas *et al*., 1997). This sheds light on a particular interaction between K19 and the actin network that could be linked with the interaction that we demonstrate between plastin 1 and K19. The interaction of calponin homology (CH) domain-containing proteins with intermediate filaments is emerging as a common theme, enlightening a role for this CH family in the establishment of boundaries between intermediate filaments and actin (Chang and Goldman, 2004). In particular, plastin 2 forms a complex with vimentin tetramers that is important for the assembly of the vimentin cytoskeleton during cell adhesion. The first CH domain of plastin 2 has been identified as the domain participating in the interaction with vimentin (Correia *et al*., 1999; Delanote *et al*., 2005). For dystrophin, another CH domain protein, an interaction of the actin-binding domain with K19 has been reported in vitro (Stone *et al*., 2005).

Loss of Plastin 1 Results in Fragility of the Intestinal Epithelium

The profound alterations of the TW must explain the sensitivity of the BB of *Pls1*$^{-/-}$ mice to the mechanical stress applied during biochemical isolation. A decreased stability of the BB has been reported in myosin 1a-deficient mice and in myosin 1B-deficient *Drosophila melanogaster* that has been related to a decreased calcium-buffering activity (Tyska *et al*., 2005; Hegan *et al*., 2007). The loss of this buffering activity would result in increased actin filament severing by villin. Although plastin 1 is capable of binding calcium ions through its N-terminal EF hands (Lin *et al*., 1994), it is not as

abundant as class I myosins; therefore, no major influence on the calcium concentration is to be expected in the BBs of the *Pls1*$^{-/-}$ mouse. Carbachol treatment and fasting/refeeding, two situations that provoke elevated intracellular calcium levels, have also revealed that the plastin 1 deficiency does not affect the severing activity of villin (data not shown).

A major consequence of the altered structural integrity of the BB in the *Pls1*$^{-/-}$ mice is the decreased transepithelial resistance of the intestine despite apparently normal structure and protein composition of the adhesion complex. *Pls1*$^{-/-}$ mice are also more sensitive to DSS-induced colitis, in agreement with the increased fragility of the apical pole. Higher sensitivity to DSS treatment occurs in villin-deficient mice that recent studies attribute to the loss of the antiapoptotic activity of this protein leading to an imbalance between cell renewal and apoptosis (Ferrary *et al*., 1999; Wang *et al*., 2008). Although it is not clear why *Pls1*$^{-/-}$ female mice die significantly earlier than the males upon DSS treatment, a possible explanation may be the different cell renewal rates between males and females. Indeed, BALB/c females are more resistant to parasitic infections because of a higher cell renewal rate allowing a faster expulsion of the parasites (Bancroft *et al*., 2000; Cliffe *et al*., 2005). We speculate that in the females, contrary to the males, the cell renewal rate cannot increase further under stress situations, making them more sensitive. An alternative explanation could be the well documented differences in the immunological response between males and females (Schuurs and Verheul, 1990), which would fit well with the increased scores of inflammatory response observed in the *Pls1*$^{-/-}$ females.

Because *Pls1*$^{-/-}$ mice do not display an overt phenotype, the increased fragility of the BB and the increased rate of cell death could be balanced by the elevated rate of cell migration. A possible explanation for the lack of evidence of an increased number of proliferating cells in the crypts of the *Pls1*$^{-/-}$ mice is a shortening of the cell cycle of the stem cell population as reported for example after gamma or beta irradiation of the intestine (Tsubouchi and Potten, 1985).

In summary, the absence of plastin 1 strongly affects the cohesion of the apical pole probably by the loss of an anchorage between the different cytoskeletal networks. This destabilization must be responsible for the enhanced fragility of the whole epithelium when challenged. Plastin 1 thus is a major player in the integrity of the intestinal barrier.

ACKNOWLEDGMENTS

We are grateful to Mark Mooseker (Yale School of Medicine, New Haven, CT), Marie-Christine Lecomte (INSERM U665, Paris, France), Ahmed Zahraoui (Institut Curie, Paris, France), and Detlev Drenckhahn (University of Würzburg, Würzburg, Germany) for supplying antibodies. We thank Graça Raposo for fruitful discussions and collaboration for the TEM, Sophie Kerneis for the SEM, Wieslaw Krzyzak and Alexandra Ley for excellent technical assistance, and Klaus-Peter Janssen for discussions. We acknowledge Trans-Cell-Lab Laboratory, Faculty of Medicine Xavier Bichat, Université Paris Diderot-Paris 7 (Paris, France) for the Ussing chamber analysis. This work was supported by grants of the Deutsche Forschungsgemeinschaft (RI 1034/5), the Köln Fortune Program of the Medical Faculty, University of Cologne, and the Medical Research Council (87863) (to F. R.), and the Curie Institute Foundation (to S.Ro.). E.-M.S.G.-G. was funded in part by a fellowship from the Köln Fortune Program. C. R. was funded by a fellowship from the Association pour la Recherche contre le Cancer. S.Ra. was funded by a fellowship from the Fundación Ramón Areces.

REFERENCES

Ameen, N. A., Figueroa, Y., and Salas, P. J. (2001). Anomalous apical plasma membrane phenotype in CK8-deficient mice indicates a novel role for intermediate filaments in the polarization of simple epithelia. J. Cell Sci. *114*, 563–575.

Arpin, M., Friederich, E., Algrain, M., Vernel, F., and Louvard, D. (1994). Functional differences between L- and T-plastin isoforms. J. Cell Biol. *127*, 1995–2008.

Athman, R., Louvard, D., and Robine, S. (2002). The epithelial cell cytoskeleton and intracellular trafficking. III. How is villin involved in the actin cytoskeleton dynamics in intestinal cells? Am. J. Physiol. Gastrointest. Liver Physiol. *283*, G496–G502.

Bancroft, A. J., Artis, D., Donaldson, D. D., Sypek, J. P., and Grencis, R. K. (2000). Gastrointestinal nematode expulsion in IL-4 knockout mice is IL-13 dependent. Eur. J. Immunol. *30*, 2083–2091.

Baribault, H., Penner, J., Iozzo, R. V., and Wilson-Heiner, M. (1994). Colorectal hyperplasia and inflammation in keratin 8-deficient FVB/N mice. Genes Dev. *8*, 2964–2973.

Bartles, J. R., Zheng, L., Li, A., Wierda, A., and Chen, B. (1998). Small espin: a third actin-bundling protein and potential forked protein ortholog in brush border microvilli. J. Cell Biol. *143*, 107–119.

Bement, W.M., and Mooseker, M.S. (1996). The cytoskeleton of the intestinal epithelium: components, assembly, and dynamic rearrangements. In: The Cytoskeleton, vol. 3, ed. J. E. Hesketh and I. F. Pryme, Greenwich, CT: JAI Press, 359–404.

Bretscher, A. (1983). Purification of an 80,000-dalton protein that is a component of the isolated microvillus cytoskeleton, and its localization in nonmuscle cells. J. Cell Biol. *97*, 425–432.

Bretscher, A., and Weber, K. (1978). Localization of actin and microfilament-associated proteins in the microvilli and terminal web of the intestinal brush border by immunofluorescence microscopy. J. Cell Biol. *79*, 839–845.

Bretscher, A., and Weber, K. (1979). Villin: the major microfilament-associated protein of the intestinal microvillus. Proc. Natl. Acad. Sci. USA *76*, 2321–2325.

Bretscher, A., and Weber, K. (1980). Fimbrin, a new microfilament-associated protein present in microvilli and other cell surface structures. J. Cell Biol. *86*, 335–340.

Broschat, K. O., Weber, A., and Burgess, D. R. (1989). Tropomyosin stabilizes the pointed end of actin filaments by slowing depolymerization. Biochemistry *28*, 8501–8506.

Chafel, M. M., Shen, W., and Matsudaira, P. (1995). Sequential expression and differential localization of I-, L-, and T-fimbrin during differentiation of the mouse intestine and yolk sac. Dev. Dyn. *203*, 141–151.

Chang, L., and Goldman, R. D. (2004). Intermediate filaments mediate cytoskeletal crosstalk. Nat. Rev. Mol. Cell Biol. *5*, 601–613.

Chen, H., *et al*. (2003). Role for plastin in host defense distinguishes integrin signaling from cell adhesion and spreading. Immunity *19*, 95–104.

Cliffe, L. J., Humphreys, N. E., Lane, T. E., Potten, C. S., Booth, C., and Grencis, R. K. (2005). Accelerated intestinal epithelial cell turnover: a new mechanism of parasite expulsion. Science *308*, 1463–1465.

Correia, I., Chu, D., Chou, Y. H., Goldman, R. D., and Matsudaira, P. (1999). Integrating the actin and vimentin cytoskeletons. adhesion-dependent formation of fimbrin-vimentin complexes in macrophages. J. Cell Biol. *146*, 831–842.

Costa de Beauregard, M. A., Pringault, E., Robine, S., and Louvard, D. (1995). Suppression of villin expression by antisense RNA impairs brush border assembly in polarized epithelial intestinal cells. EMBO J. *14*, 409–421.

Crosnier, C., Stamataki, D., and Lewis, J. (2006). Organizing cell renewal in the intestine: stem cells, signals and combinatorial control. Nat. Rev. Genet. *7*, 349–359.

Dalby-Payne, J. R., O'Loughlin, E. V., and Gunning, P. (2003). Polarization of specific tropomyosin isoforms in gastrointestinal epithelial cells and their impact on CFTR at the apical surface. Mol. Biol. Cell *14*, 4365–4375.

Daudet, N., and Lebart, M. C. (2002). Transient expression of the t-isoform of plastins/fimbrin in the stereocilia of developing auditory hair cells. Cell Motil. Cytoskeleton *53*, 326–336.

Delanote, V., Vandekerckhove, J., and Gettemans, J. (2005). Plastins: versatile modulators of actin organization in (patho)physiological cellular processes. Acta Pharmacol. Sin. *26*, 769–779.

Dieleman, L. A., Palmen, M. J., Akol, H., Bloemena, E., Peña, A. S., Meuwissen, S. G., and Van Rees, E. P. (1998). Chronic experimental colitis induced by dextran sulphate sodium (DSS) is characterized by Th1 and Th2 cytokines. Clin. Exp. Immunol. *114*, 385–391.

Ezzell, R. M., Chafel, M. M., and Matsudaira, P. T. (1989). Differential localization of villin and fimbrin during development of the mouse visceral endoderm and intestinal epithelium. Development *106*, 407–419.

Fath, K. R., Obenauf, S. D., and Burgess, D. R. (1990). Cytoskeletal protein and mRNA accumulation during brush border formation in adult chicken enterocytes. Development *109*, 449–459.

Ferrary, E., *et al*. (1999). In vivo, villin is required for Ca^{2+}-dependent F-actin disruption in intestinal brush borders. J. Cell Biol. *146*, 819–830.

Friederich, E., Pringault, E., Arpin, M., and Louvard, D. (1990). From the structure to the function of villin, an actin-binding protein of the brush border. Bioessays *12*, 403–408.

Friederich, E., Vancompernolle, K., Huet, C., Goethals, M., Finidori, J., Vandekerckhove, J., and Louvard, D. (1992). An actin-binding site containing a conserved motif of charged amino acid residues is essential for the morphogenic effect of villin. Cell *70*, 81–92.

Giganti, A., Plastino, J., Janji, B., Van Troys, M., Lentz, D., Ampe, C., Sykes, C., and Friederich, E. (2005). Actin-filament cross-linking protein T-plastin increases Arp2/3-mediated actin-based movement. J. Cell Sci. *118*, 1255–1265.

Glenney, J. R., Jr., Glenney, P., Osborn, M., and Weber, K. (1982). An F-actin- and calmodulin-binding protein from isolated intestinal brush borders has a morphology related to spectrin. Cell *28*, 843–854.

Glenney, J. R., Jr., Kaulfus, P., Matsudaira, P., and Weber, K. (1981). F-actin binding and bundling properties of fimbrin, a major cytoskeletal protein of microvillus core filaments. J. Biol. Chem. *256*, 9283–9288.

Hegan, P. S., Mermall, V., Tilney, L. G., and Mooseker, M. S. (2007). Roles for *Drosophila melanogaster* myosin IB in maintenance of enterocyte brush-border structure and resistance to the bacterial pathogen *Pseudomonas entomophila*. Mol. Biol. Cell *18*, 4625–4636.

Heintzelman, M. B., Hasson, T., and Mooseker, M. S. (1994). Multiple unconventional myosin domains of the intestinal brush border cytoskeleton. J. Cell Sci. *107*, 3535–3543.

Hirokawa, N., Cheney, R. E., and Willard, M. (1983). Location of a protein of the fodrin-spectrin-TW260/240 family in the mouse intestinal brush border. Cell *32*, 953–965.

Hirokawa, N., Tilney, L. G., Fujiwara, K., and Heuser, J. E. (1982). Organization of actin, myosin, and intermediate filaments in the brush border of intestinal epithelial cells. J. Cell Biol. *94*, 425–443.

Keller, T. C., 3rd, Conzelman, K. A., Chasan, R., and Mooseker, M. S. (1985). Role of myosin in terminal web contraction in isolated intestinal epithelial brush borders. J. Cell Biol. *100*, 1647–1655.

Laird, P. W., Zijderveld, A., Linders, K., Rudnicki, M. A., Jaenisch, R., and Berns, A. (1991). Simplified mammalian DNA isolation procedure. Nucleic Acids Res. *19*, 4293.

Lin, C. S., Aebersold, R. H., Kent, S. B., Varma, M., and Leavitt, J. (1988). Molecular cloning and characterization of plastin, a human leukocyte protein expressed in transformed human fibroblasts. Mol. Cell. Biol. *8*, 4659–4668.

Lin, C. S., Park, T., Chen, Z. P., and Leavitt, J. (1993). Human plastin genes. Comparative gene structure, chromosome location, and differential expression in normal and neoplastic cells. J. Biol. Chem. *268*, 2781–2792.

Lin, C. S., Shen, W., Chen, Z. P., Tu, Y. H., and Matsudaira, P. (1994). Identification of I-plastin, a human fimbrin isoform expressed in intestine and kidney. Mol. Cell. Biol. *14*, 2457–2467.

Loomis, P. A., Zheng, L., Sekerkova, G., Changyaleket, B., Mugnaini, E., and Bartles, J. R. (2003). Espin cross-links cause the elongation of microvillus-type parallel actin bundles in vivo. J. Cell Biol. *163*, 1045–1055.

Magin, T. M., Schröder, R., Leitgeb, S., Wanninger, F., Zatloukal, K., Grund, C., and Melton, D. W. (1998). Lessons from keratin 18 knockout mice: formation of novel keratin filaments, secondary loss of keratin 7 and accumulation of liver-specific keratin 8-positive aggregates. J. Cell Biol. *140*, 1441–1451.

Mashimo, H., Wu, D. C., Podolsky, D. K., and Fishman, M. C. (1996). Impaired defense of intestinal mucosa in mice lacking intestinal trefoil factor. Science *274*, 262–565.

Matsudaira, P., Mandelkow, E., Renner, W., Hesterberg, L. K., and Weber, K. (1983). Role of fimbrin and villin in determining the interfilament distances of actin bundles. Nature *301*, 209–214.

Matsudaira, P. T., and Burgess, D. R. (1979). Identification and organization of the components in the isolated microvillus cytoskeleton. J. Cell Biol. *83*, 667–673.

McConnell, R. E., and Tyska, M. J. (2007). Myosin-1a powers the sliding of apical membrane along microvillar actin bundles. J. Cell Biol. *177*, 671–681.

Mooseker, M. S. (1985). Organization, chemistry, and assembly of the cytoskeletal apparatus of the intestinal brush border. Annu. Rev. Cell Biol. *1*, 209–241.

Mooseker, M. S., and Tilney, L. G. (1975). Organization of an actin filament-membrane complex. Filament polarity and membrane attachment in the microvilli of intestinal epithelial cells. J. Cell Biol. *67*, 725–743.

Nakano, K., Satoh, K., Morimatsu, A., Ohnuma, M., and Mabuchi, I. (2001). Interactions among a fimbrin, a capping protein, and an actin-depolymerizing factor in organization of the fission yeast actin cytoskeleton. Mol. Biol. Cell *12*, 3515–3526.

Percival, J. M., Thomas, G., Cock, T. A., Gardiner, E. M., Jeffrey, P. L., Lin, J. J., Weinberger, R. P., and Gunning, P. (2000). Sorting of tropomyosin isoforms in synchronised NIH 3T3 fibroblasts: evidence for distinct microfilament populations. Cell Motil. Cytoskeleton *47*, 189–208.

Pinson, K. I., Dunbar, L., Samuelson, L., and Gumucio, D. L. (1998). Targeted disruption of the mouse villin gene does not impair the morphogenesis of microvilli. Dev. Dyn. *211*, 109–121.

Prost, J., Barbetta, C., and Joanny, J. F. (2007). Dynamical control of the shape and size of stereocilia and microvilli. Biophys. J. *93*, 1124–1133.

Salas, P. J., Rodriguez, M. L., Viciana, A. L., Vega-Salas, D. E., and Hauri, H. P. (1997). The apical submembrane cytoskeleton participates in the organization of the apical pole in epithelial cells. J. Cell Biol. *137*, 359–375.

Sambrook, J., David, J., and Russell, W. (2001). Molecular Cloning: A Laboratory Manual, Cold Spring Harbor, NY: Cold Spring Harbor Laboratory Press.

Saotome, I., Curto, M., and McClatchey, A. I. (2004). Ezrin is essential for epithelial organization and villus morphogenesis in the developing intestine. Dev. Cell *6*, 855–864.

Schuurs, A. H., and Verheul, H. A. (1990). Effects of gender and sex steroids on the immune response. J. Steroid Biochem. *35*, 157–172.

Stone, M. R., O'Neill, A., Catino, D., and Bloch, R. J. (2005). Specific interaction of the actin-binding domain of dystrophin with intermediate filaments containing keratin 19. Mol. Biol. Cell *16*, 4280–4293.

Tamai, Y., Ishikawa, T., Bosl, M. R., Mori, M., Nozaki, M., Baribault, H., Oshima, R. G., and Taketo, M. M. (2000). Cytokeratins 8 and 19 in the mouse placental development. J. Cell Biol. *151*, 563–572.

Tilney, L. G., Connelly, P. S., Ruggiero, L., Vranich, K. A., and Guild, G. M. (2003). Actin filament turnover regulated by cross-linking accounts for the size, shape, location, and number of actin bundles in *Drosophila* bristles. Mol. Biol. Cell *14*, 3953–3966.

Tilney, L. G., Tilney, M. S., and DeRosier, D. J. (1992). Actin filaments, stereocilia, and hair cells: how cells count and measure. Annu. Rev. Cell Biol. *8*, 257–274.

Tilney, M. S., Tilney, L. G., Stephens, R. E., Merte, C., Drenckhahn, D., Cotanche, D. A., and Bretscher, A. (1989). Preliminary biochemical characterization of the stereocilia and cuticular plate of hair cells of the chick cochlea. J. Cell Biol. *109*, 1711–1723.

Tsubouchi, S., and Potten, C. S. (1985). Recruitment of cells in the small intestine into rapid cell cycle by small doses of external gamma or internal beta radiation. Int. J. Radiat. Biol. Relat. Stud. Phys. Chem. Med. *43*, 361–369.

Tyska, M. J., Mackey, A. T., Huang, J. D., Copeland, N. G., Jenkins, N. A., and Mooseker, M. S. (2005). Myosin-1a is critical for normal brush border structure and composition. Mol. Biol. Cell *16*, 2443–2457.

Wald, F. A., Oriolo, A. S., Casanova, M. L., and Salas, P. J. (2005). Intermediate filaments interact with dormant ezrin in intestinal epithelial cells. Mol. Biol. Cell *16*, 4096–4107.

Wang, Y., Srinivasan, K., Siddiqui, M. R., George, S. P., Tomar, A., and Khurana, S. (2008). A novel role for villin in intestinal epithelial cell survival and homeostasis. J. Biol. Chem. *283*, 9454–9464.

Weiser, M. M. (1973). Intestinal epithelial cell surface membrane glycoprotein synthesis. I. An indicator of cellular differentiation. J. Biol. Chem. *248*, 2536–2541.

Zheng, L., Sekerkova, G., Vranich, K., Tilney, L. G., Mugnaini, E., and Bartles, J. R. (2000). The deaf jerker mouse has a mutation in the gene encoding the espin actin-bundling proteins of hair cell stereocilia and lacks espins. Cell *102*, 377–385.

Zigmond, S. H., Furukawa, R., and Fechheimer, M. (1992). Inhibition of actin filament depolymerization by the *Dictyostelium* 30,000-D actin-bundling protein. J. Cell Biol. *119*, 559–567.